

Effect of Red Cell Clustering and Anisotropy on Ultrasound Blood Backscatter: A Monte Carlo Study

David Savéry and Guy Cloutier, *Member, IEEE*

Abstract—When flowing at a low shear rate, blood appears hyperechogenic on ultrasound B-scans. The formation of red blood cell (RBC) aggregates that also alters blood viscosity is the microscopic mechanism explaining this acoustical phenomenon. In this study, Monte Carlo simulations were performed to predict how RBC clustering increases ultrasound scattering by blood. A bidimensional Gibbs-Markov random point process parameterized by the adhesion energy ϵ and an anisotropy index ν was used to describe RBC positions for a hematocrit $H = 40\%$. The frequency dependence of the backscattering coefficient $\chi(f)$ was computed using Born approximation. The backscattering coefficient χ^0 at 5 MHz and the spectral slopes n_x and n_y ($\chi \propto f^{n_x}$ or f^{n_y}) measured, respectively, when theinsonification is parallel and perpendicular with the RBC cluster axis were then extracted. Under isotropic conditions, χ^0 increased up to 7 dB with ϵ and $n_x = n_y$ decreased from 4.2 to 3.4. Under anisotropic conditions, the backscattering was stronger perpendicularly to aggregate axis, resulting in $n_x < n_y$. The anisotropy in scattering appeared more pronounced when ϵ or ν increased. These two dimensional results generally predict that low-frequency blood backscatter is related to cluster dimension, and higher-frequency properties are affected by finer morphological features as anisotropy. This numerically establishes that ultrasound backscatter spectroscopy on a large frequency range is pertinent to characterize in situ hemorheology.

I. INTRODUCTION

ULTRASONIC tissue characterization (UTC) techniques (see Table I for list of symbols and abbreviations) aim at diagnosing the pathophysiological state of the imaged tissues by detecting abnormalities in their acoustical properties (as backscatter, attenuation, or speed of sound) [1]. Although textured B-scan images are commonly used to

Manuscript received December 23, 2003; accepted August 5, 2004. This work was supported by the Institutes of Health Research of Canada (# MOP-36467). The salaries of both investigators were partially supported by a studentship from the Groupe de Recherche en modélisation biomédicale de FCAR (Québec funding agency, DS.) and by a National Scientist award from the Fonds de la Recherche en Santé du Québec, GC.

G. Cloutier is with the Laboratory of Biorheology and Medical Ultrasonics, Research Center, University of Montréal Hospital, Montréal, Québec, H2L 2W5, Canada, and Department of Radiology, Radio-oncology and Nuclear Medicine, University of Montréal, Montréal, Québec, H3C 3J7, Canada (e-mail: guy.cloutier@umontreal.ca).

At the time of this research, D. Savéry was with the Laboratory of Biorheology and Medical Ultrasonics, University of Montréal Hospital, Montréal, Québec, Canada. He is now with Philips Research USA, Healthcare Systems and Information Technology Department, Briarcliff Manor, NY (e-mail: david.savery@philips.com).

provide anatomical information, UTC measures complementary indices by mapping the scattering and absorption properties of tissues. Biophysical and biochemical activities of the organs were shown to affect these quantitative acoustic features. Cell apoptosis [2], myocardium ischemia [3], or osteoporotic loss of bone [4] are examples of pathological events that could potentially be investigated by these means.

In this paper, the sensitivity of blood scattering properties to the erythrocyte aggregation state is investigated. It represents a typical application of UTC for measuring ensemble-averaged macroscopic manifestations of microscopic phenomena occurring at a scale under the resolution of commercial ultrasound (US) imaging systems. In the presence of plasmatic proteins such as fibrinogen and at a low shear rate, red blood cells (RBCs) physiologically form aggregates or rouleaux [5], [6]. The RBC clustering dramatically affects blood rheology [7], blood echogenicity [8], and many other blood physical properties (e.g., optical [9] or dielectric [10]). An abnormal level of RBC aggregation may have pathological consequences: the increase of blood viscosity perturbs microcirculatory hemodynamics [11], influences the peripheral resistance [12], and correlates with risks of cardiovascular disease [13]. The in vivo measurement of US blood backscatter would enable one to detect RBC aggregation and the related blood rheology impairments. Its quantification would help to elucidate how hemorheology is involved in the etiology of cardiovascular diseases.

The frequency dependence of the backscattering coefficient $\chi = \chi(f)$ is commonly used as the characteristic US signature of a tissue [1]. In the range of acoustical frequencies covered by medical US transducers (typically 1–40 MHz), a power law $\chi/\chi^0 = (f/f_0)^n$ is often accurate enough to quantify this dependence. In this spectroscopic analysis, f_0 is a chosen reference frequency (here $f_0 = 5$ MHz) and $\{\chi^0, n\}$ are tissue acoustic characteristics. Many experiments have shown that blood exposed to a high shear rate behaves as a Rayleigh scattering tissue. For instance, by using the same data reduction to results by Foster *et al.* [14], one finds $\chi^0 = 1.3 \times 10^{-3} \text{ m}^{-1} \cdot \text{Sr}^{-1}$, $n = 3.5$ for a shear rate $\dot{\gamma} = 32 \text{ s}^{-1}$. Non-Rayleigh effects arise at a low shear rate when RBCs aggregate: $\chi^0 = 2.8 \text{ m}^{-1} \cdot \text{Sr}^{-1}$ and $n = 0.4$ for $\dot{\gamma} = 0.16 \text{ s}^{-1}$. However, the sensitivity of parameters $\{\chi^0, n\}$ to the erythrocyte aggregation level remains poorly documented. Moreover, other Doppler experimental studies (as in Allard *et*

TABLE I
LIST OF SYMBOLS AND ABBREVIATIONS.

a	major axis of the interaction ellipse
b	minor axis of the interaction ellipse
c	speed of sound = 1540 m.s ⁻¹
χ	blood backscattering coefficient
χ_{ref}	reference backscattering coefficient (5 MHz, no aggregation)
$\chi^0, \chi_x^0, \chi_y^0$	blood backscattering coefficient at 5 MHz
δ	Dirac function
Δk	sampling interval of the wave vector dependent $S(-2\vec{k})$
$E[X]$	ensemble average of a random variable X
ϵ	aggregation energy
f	acoustical frequency
f_0	reference 5 MHz frequency
$\phi(u)$	$1/\pi \times$ intersection area of two unit disks separated by $2u$
$\dot{\gamma}$	shear rate
γ_z	acoustic impedance contrast between RBCs and plasma
$\vec{h} = (h_x, h_y)$	intercellular lag
H	hematocrit
$i = \sqrt{-1}$	imaginary number
$I_{[Q]}$	indicator function = 1 if Q is true, = 0 if Q is false
I, i	indices
j	index
J_1	first order Bessel function of the first kind
\vec{k}	incident acoustic wave vector
k_B	Boltzmann constant
L	square basis of V
ℓ	index
λ_0	surface index of the interaction ellipse
m	erythrocyte number density
M_i	total number of Metropolis steps
n, n_x, n_y	acoustic spectral slopes
N	number of erythrocytes in V
$N_{\Omega}(\vec{r})$	microscopic number density
N_{ij}	matrix of density inside V
N_p^2	size of N_{ij}
ν	anisotropy index of the interaction ellipse
Ox	long axis direction of the interaction ellipse
Oy	short axis direction of the interaction ellipse
$\xi = (\vec{x}_1, \dots, \vec{x}_N), \omega_i$	configuration
Ω	random point process
p	uniform random number $\in [0; 1]$
P	probability
$p_{\Omega}(\xi)$	probability density function of Ω
$\vec{q} = -2\vec{k}$	acoustic scattering vector
$q = \exp(-\Delta U/k_B T)$	Metropolis ratio
R	red blood cell radius
\vec{r}	current point in V
RBC	red blood cell
$S(\vec{q})$	structure factor
$\sigma_b(\vec{k})$	erythrocyte cross-section
σ_b^0	erythrocyte cross-section at 5 MHz
T	temperature
$U_{\Omega}(\xi)$	total configuration energy
US	ultrasound
UTC	ultrasound tissue characterization
ΔU	energy change in a Metropolis step
V	scattering region
$V_2(\vec{h})$	pair energy potential
V_{rep}	repulsion energy
V_s	RBC volume
W_0	Perkus Yevick packing factor of 2D hard disks
\vec{x}	current point in Ω
\vec{x}_{new}	new proposed position in a Monte Carlo step
Z_{Ω}	partition function

al. [15], at 10 MHz) showed that the level of backscatter was angle-dependent, which indicates non-Rayleigh scattering.

Consequently, this paper investigates the influence of RBC adhesion and medium anisotropy on $\{\chi^0, n\}$ by using computer simulations.

Bidimensional models were used in this study because of the computational difficulty to generate many-particle volumic configurations. Also restricted, this choice enabled us to extend a number of previous two-dimensional (2-D) studies by integrating more realistic microstructural (anisotropic clustering conditions) or acoustical conditions (non-Rayleigh frequencies). In [16] or in [17], the effect of the steric repulsion between RBCs was modeled in the low-frequency approximation. Both approaches successfully predicted the nonlinear dependence of the backscatter with the hematocrit as first observed in [18]. However, they did not take into consideration non-Rayleigh phenomena nor the influence of particle cluster formation on blood scattering. In [19], the backscatter by 2-D and 3-D geometric scatterer clusters was assessed in the same packing factor approximation (low frequency scattering). It showed that the backscatter increases with the (mean) number of particles per cluster. However, this approximation only applies to low frequency insonifications and only models Rayleigh scattering ($n = 4$). In [20], both the effects of flow-mediated clustering and higher frequency were taken into account using 2-D particle dynamics. Viscous forces on particles flowing in shear were empirically modeled in this study. Computational difficulties were encountered, which was barely practical as variabilities required to average numerous realizations.

As often encountered in materials microstructure numerical modeling, an alternative to molecular dynamics is to use Monte Carlo sampling techniques to simulate heterogeneous media.

Thus, in this paper we propose a novel description of RBC clustering by using a 2-D random point process approach. The microstructure created by RBC packing is described by parameters of the statistical spatial model, an adhesion energy index ϵ , and an anisotropy index ν . Monte Carlo simulations then are generated to predict the evolution of $\{\chi^0, n\}$ as a function of the aggregation state (adhesion and anisotropy statistic parameters) and of the insonification angle.

II. METHODS

Acoustical waves propagating in a linear medium are scattered when encountering density and speed of sound inhomogeneities [21]. In the context of acoustics, blood can be described roughly as a biphasic fluid composed of RBCs (volume fraction $H = 40\%$) immersed in the plasma [22], [23], which is a Newtonian fluid. Blood backscatter depends on the frequency, hematocrit, plasma, and RBC acoustical properties (density and compressibility) and on the geometry of the dense network of erythrocytes. Ad-

hesive and steric interparticle interactions affect the conformation of this viscoelastic phase. Double-layer electrostatic repulsive force is neglected here because of its small nanometric range.

In this paper, the microstructural pattern created by erythrocytes was modeled by a random Gibbs-Markov point process, as described in Section II-A. The weak scattering approximation also is adopted to simulate US backscattering by this modeled medium (Section II-B).

A. Microstructure Model

1. *Random Configuration:* A collection of $N = mV$ cylindrical RBCs (m is the spatial number density of RBCs) was randomly spread on a periodic parallelepiped of volume V . The positions of the RBC centers, noted $\xi = (\vec{x}_1, \dots, \vec{x}_N)$, jointly define a random configuration. Because of multiple intercellular interactions and hydrodynamic forces acting on cells, all configurations ξ are not equally probable. A convenient class of random point process is the Gibbs-Markov stochastic model [24]. A Gibbs-Markov point process Ω is defined by assigning an energy level $U_\Omega(\xi) = U_\Omega(\vec{x}_1, \dots, \vec{x}_N)$ to each configuration ξ of the phase space V^N . This configuration energy is supposed to be independent of the rotations of the erythrocytes and consider only two-body interactions. By writing $V_2(\vec{h})$ the pair potential that represents the interaction energy of two RBCs separated by the lag \vec{h} , one defines $U_\Omega(\xi)$ as the sum of pair energies:

$$U_\Omega(\xi) = \sum_{i < j} V_2(\vec{x}_i - \vec{x}_j). \quad (1)$$

At a fixed temperature T , the Gibbs-Markov process Ω has, by definition, a probability density function that obeys Boltzmann statistics:

$$p_\Omega(\xi) = \frac{1}{Z_\Omega} e^{-U_\Omega(\xi)/k_B T}, \quad (2)$$

where Z_Ω is the normalizing partition function, and k_B is the Boltzmann constant. Note that the Boltzmann statistics favor configurations of low energy. However, configurations with a positive infinite energy have no chance to appear. The absolute temperature controls the variability of these configurations.

The choice of $V_2(\vec{h})$ and of the number density m completely defines Ω and, therefore, all statistical properties of the spatial pattern, including the mean scattering properties of the modeled medium.

2. *Choice of Pair Potential:* When observing the spatial pattern formed by RBCs when blood flows in a stationary shear flow (velocity in the Ox direction), two microscopic features can be observed. First, RBCs do not overlap in space. Second, RBC rouleaux align along the flow streamlines, which induces structural anisotropy. This type of point configuration can be modeled by a Gibbs-Markov model with a pair potential $V_2(\vec{h})$ that has two special

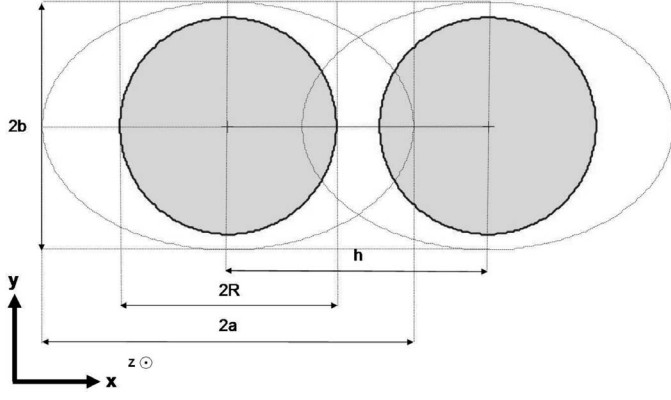


Fig. 1. Geometrical parameters of the interaction ellipse and of the forbidden circular zones used in the model of pair potential. The figure corresponds to $\nu = 0.5$ and $\lambda_0 = 0.4$.

properties. The pair potential first should be highly repulsive (positive) or even infinite (hardcore potential) when two RBCs are distant by less than a diameter. The pair potential also should be negative when RBCs are in contact and aligned with Ox to favor adhesion in this direction.

The pair potential was empirically chosen in this study to satisfy these two criteria. The expression of $V_2(\vec{h})$ was defined as follows. One considers that each RBC center is surrounded by two concentric layers (Fig. 1): a forbidden circular zone that defines the range of the steric forces (of diameter $2R$) and an elliptic attractive area. The major axis a and the minor axis b of the ellipsis, respectively, are aligned along Ox and Oy . The pair potential was defined as the sum of two energies: a repulsive positive part that arises when forbidden zones overlap, and a negative part proportional to the intersection area of the attractive zones. Quantitatively, this gives:

$$V_2(\vec{h}) = V_{rep} I_{[|\vec{h}| < 2R]} - \epsilon \phi \left(\frac{1}{2} \sqrt{\left(\frac{h_x}{a}\right)^2 + \left(\frac{h_y}{b}\right)^2} \right), \quad (3)$$

where $\phi(u)$ is the function of the real variable u ¹ defined by:

$$\phi(u) = \frac{2}{\pi} I_{[|u| < 1]} \left(\arccos u - u \sqrt{1 - u^2} \right). \quad (4)$$

In the above equations, $I_{[]}$ is the indicator function, $V_{rep} \gg \epsilon$ is a repulsion energy, a constant chosen very great, ϵ controls the adhesion strength, and R represents the RBC radius. Fig. 2 shows the energy profile of the chosen pair potential $V_2(\vec{h})$. Two nondimensional geometric parameters (λ_0, ν) are defined as follows:

$$\pi ab = \pi(1 + \lambda_0)^2 R^2, \quad (5)$$

$$a = (1 + \nu)b. \quad (6)$$

¹The intersection of two identical ellipses with parallel axes (a, b) and centers separated by the lag $\vec{h} = (h_x, h_y)$ has the area $\pi ab \phi \left(\sqrt{h_x^2/a^2 + h_y^2/b^2}/2 \right)$.

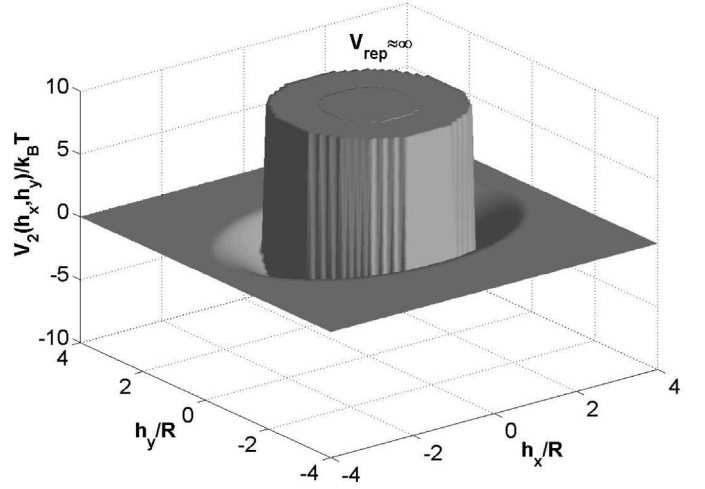


Fig. 2. Energy profile of the pair potential $V_2(\vec{h})$. The figure corresponds to $\nu = 0.5$, $\lambda_0 = 0.4$ and $\epsilon = k_B T$.

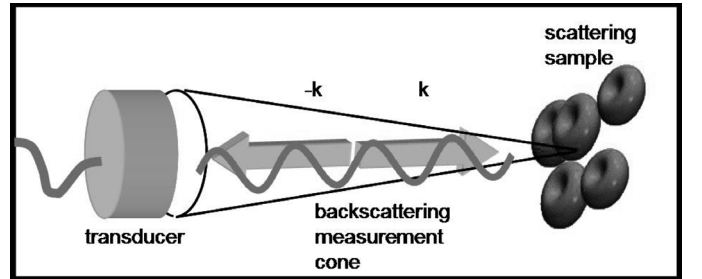


Fig. 3. Schematic description of the scattering experiment.

They, respectively, represent the reduced area of the attractive zone and the excess of the major on the minor axis. The condition $\nu = 0$ corresponds to an isotropic medium.

B. Scattering Model

The ability of a tissue to generate acoustical echoes (Fig. 3) is often quantified by the frequency-dependent backscattering coefficient χ [1]. For a heterogenous material composed of weak scattering particles, the expression of the backscattering coefficient can be factorized [25], [26] under the form:

$$\chi(\vec{k}) = m S(-2\vec{k}) \sigma_b(\vec{k}), \quad (7)$$

where \vec{k} is the incident wave vector ($k = 2\pi f/c$, where f is the acoustical frequency and $c \sim 1540 \text{ m.s}^{-1}$ is the bulk sound speed) and $\sigma_b(\vec{k})$ is the backscattering cross section of a single scatterer. The function $S(\vec{q})$ is the mean structure factor [17] of the random configuration Ω of N points, defined for a given scattering vector $\vec{q} = -2\vec{k}$ (noting $i = \sqrt{-1}$) by:

$$S(\vec{q}) = E \left[\frac{1}{N} \left| \sum_{\vec{x} \in \Omega} e^{-i\vec{q} \cdot \vec{x}} \right|^2 \right]. \quad (8)$$

The structure factor quantifies the effect of the spatial random organization of the scatterers on the backscattering coefficient. For independent scatterers (i.e., when Ω is a spatial homogeneous Poisson point process) $S(\vec{q}) \equiv 1$. The backscattering cross section $\sigma_b(\vec{k})$ can be defined as the area of the perfect plane reflector that backscatters as much power as an isolated RBC. In this study, RBCs were modeled as parallel weak scattering cylinders of radius R and volume V_s , that have a small acoustical impedance contrast (relatively to the plasma) $\langle \gamma_z \rangle = 0.11$. This assumption enables one to apply the Born approximation [21] to analytically derive the cross-section perpendicularly to their axis Oz [27]:

$$\sigma_b(\vec{k}) = \frac{1}{4\pi^2} k^4 V_s^2 \langle \gamma_z \rangle^2 \left(\frac{J_1(2kR)}{kR} \right)^2, \quad (9)$$

where J_1 is the first order Bessel function of the first kind.

C. Monte Carlo Simulation Technique

The computation of the backscattering coefficient requires the knowledge of the structure factor (7), which is by definition the expectation of a statistical quantity [as given by (8)]. Theoretically, the computation of this mean could be performed as the probability density function p_Ω of the random point process can be known via (2).

However, this calculus is completely intractable; only statistical estimations from average quantities are practically feasible in this many-particle problem. If many simulations of the random point process Ω can be generated, then a simple averaging of all the obtained sample structure factors can give an estimated value of the structure factor $S(\vec{q})$. The classical Metropolis sampler [28] was the adopted algorithm to simulate some realizations of the point process Ω .

This Monte Carlo sampling technique consists in a random walk $(\xi_0, \dots, \xi_n, \dots)$ in the phase space V^N that starts from a configuration ξ_0 and asymptotically reaches a random sample of Ω . The following iterative procedure was used for a step (ℓ) to $(\ell + 1)$, considering that the current configuration is $\xi_\ell = (\vec{x}_1^{(\ell)}, \dots, \vec{x}_N^{(\ell)})$:

- pick at random the particle labelled I uniformly in $\{1, \dots, N\}$ located in $\vec{x}_I^{(\ell)}$,
- a new position \vec{x}_{new} is chosen for I uniformly at random in V ,
- compute the energy change ΔU of the total energy U_Ω , due to a displacement of the particle I from $\vec{x}_I^{(\ell)}$ to \vec{x}_{new} , assuming that V has periodic boundaries,
- define the Metropolis ratio $q = \exp(-\Delta U/k_B T)$,
- generate a uniform random quantity $p \in [0, 1]$,
- if $p \leq q$ then $\vec{x}_I^{(\ell+1)} = \vec{x}_{new}$ else $\vec{x}_I^{(\ell+1)} = \vec{x}_I^{(\ell)}$,
- other positions remain unchanged and $\xi_{\ell+1} = (\vec{x}_1^{(\ell)}, \dots, \vec{x}_I^{(\ell+1)}, \dots, \vec{x}_N^{(\ell)})$.

Values of the different simulation parameters used in the study are given in Table II. A number $M_i = 40N$

TABLE II
MONTE CARLO SIMULATION PARAMETERS.

R	3.5 μm
λ_0	0.4
N	815
L	280 μm
M_i	32600
c	1540 m.s^{-1}
V_{rep}	$10^6 k_B T$

Metropolis steps was assumed sufficient to obtain a sample Ω of the random point process. For each simulation, a matrix N_{ij} was computed by dividing the square simulation plane L^2 in N_p^2 pixels and by counting the number of particles N_{ij} falling into each pixel (i, j) . This matrix was used for the computation of the structure factor as follows. The array N_{ij} represents a sampling of the microscopic density $N_\Omega(\vec{r})$, defined by:

$$N_\Omega(\vec{r}) = \sum_{\vec{x} \in \Omega} \delta(\vec{r} - \vec{x}), \quad (10)$$

where δ is the spatial Dirac function, and \vec{r} is the current point inside V . According to (8), the structure factor is related to the Fourier power spectrum of the random microscopic density:

$$S(\vec{q}) = E \left[\frac{1}{N} \left| \int_V N_\Omega(\vec{r}) e^{-i\vec{q} \cdot \vec{r}} d^2 r \right|^2 \right]. \quad (11)$$

Therefore, the structure factor was computed by averaging 2-D fast Fourier transforms (FFT) of the density matrix N_{ij} . This FFT gave the structure factor values $S(-2\vec{k})$ on a centered grid of wavevectors, regularly spaced by $\Delta k = \pi/L$ and with extreme wavenumber values $\pm \pi N_p / 2L$. The backscattering coefficient was assessed on each pixel of the wavevector grid using the structure factor values and (7) and (9).

D. Data Reduction and Tissue Acoustic Properties

After the function $\chi(\vec{k})$ was estimated, the amount of backscatter data characterizing the frequency dependence was reduced by computing four UTC parameters that summarize the frequency and angular dependencies of χ on the frequency range 0–40 MHz. These data $(\chi_x^0, \chi_y^0, n_x, n_y)$ were obtained by performing two power-law regressions along the two orthogonal principal directions (Ox) and (Oy):

$$\chi(k_x \vec{e}_x) = \chi_x^0 (k_x/k_0)^{n_x}, \quad (12)$$

$$\chi(k_y \vec{e}_y) = \chi_y^0 (k_y/k_0)^{n_y}. \quad (13)$$

A reference backscattering level at $f_0 = c_0 k_0 / 2\pi = 5$ MHz, χ_{ref} , was defined by the formula $\chi_{ref} = m W_0 \sigma_b^0 = 2.84 \times 10^{-4} \text{ m}^{-1} \cdot \text{Sr}^{-1}$.

In this equation, $W_0 = (1-H)^3 / (1+H)$ is the so-called Percus-Yevick packing factor [26] for 2-D hard disks and

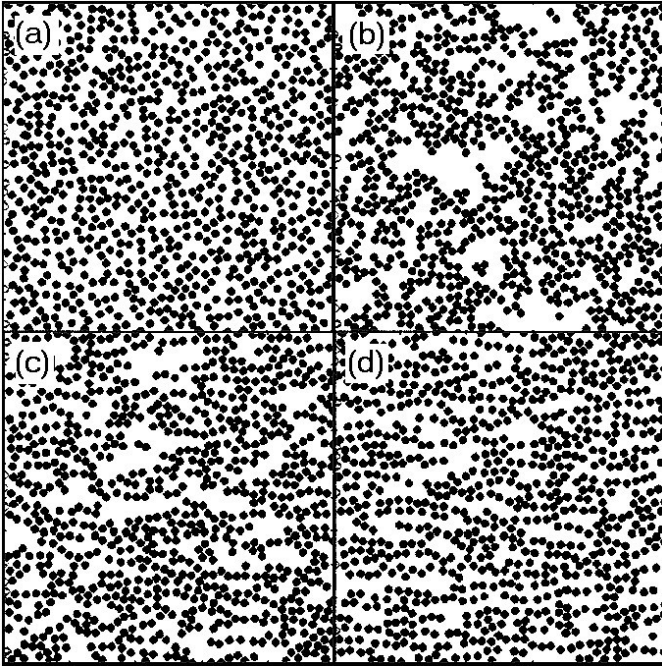


Fig. 4. Realizations of the random point process Ω for different statistical parameters. From upper left to bottom right: (a) $\epsilon = 0$, $\nu = 0$, (b) $\epsilon = 150k_B T$, $\nu = 0$, (c) $\epsilon = 50k_B T$, $\nu = 0.5$, (d) $\epsilon = 150k_B T$, $\nu = 1$.

volumic fraction $H = 0.4$, and σ_b^0 is the RBC cross section at 5 MHz, computed using (9). This quantity W_0 is the low-frequency limit of the structure factor of a suspension of nonoverlapping rigid disks. Shung *et al.* [29] experimentally demonstrated that the backscattering coefficient (and its hematocrit dependence) of nonaggregating RBC suspensions could be described by the hard sphere (3-D) Percus-Yevick formula [30]. Consequently, it seems legitimate that the Percus-Yevick approach could be applied in this 2-D study.

III. RESULTS

A. Spatial Pattern of Aggregated Cells

The growth, orientation, and organization of RBC clusters in response to different aggregation conditions can be visualized on Fig. 4. One realization of the point process is represented for selected values of (ϵ, ν) . The steric repulsion has a clear impact on the particle spatial organization. Increasing ϵ results in cluster growth, but ν modulates structure anisotropy, not independently of the cluster size. When ν deviates from zero, RBCs form aligned layers of linear clusters, but when $\nu = 0$, no particular growth direction is favored, which creates compact erythrocyte clumps.

B. Backscatter and Frequency Dependence

Variations of the mean backscattering coefficient in the frequency range 0–130 MHz are given on Fig. 5. The backscattering coefficient increases with the frequency, but

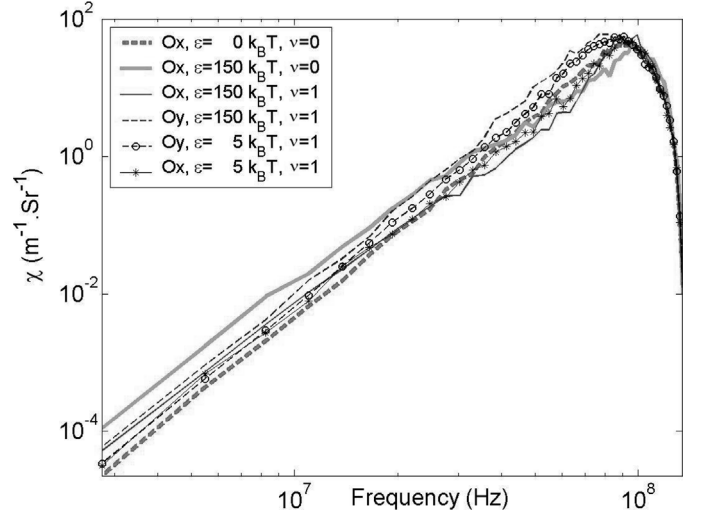


Fig. 5. Frequency dependence of the mean backscattering coefficient for different aggregation conditions (ϵ , aggregation energy; ν , anisotropy index) and insonification angles (Ox , cluster long axis, Oy , perpendicular axis). No standard errors are shown for clarity.

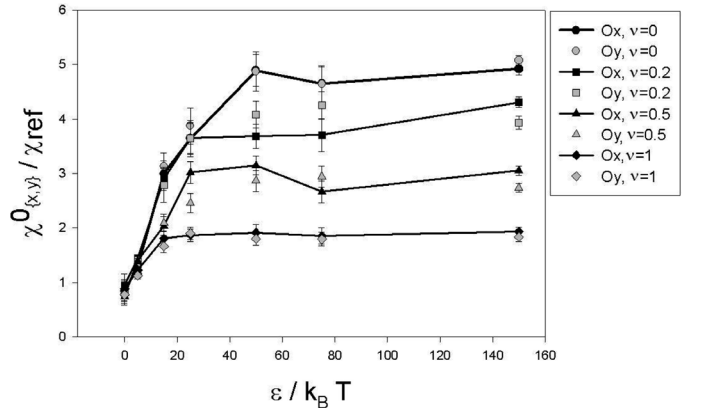


Fig. 6. Normalized backscattering coefficient at 5 MHz, in perpendicular (Oy) and in parallel (Ox) with the growth axis as a function of the aggregation potential ϵ and of the anisotropy index ν . The error bars represent the standard error of the mean.

at a rate that is specific to the RBC microstructure variables (ϵ, ν) and to the insonifying angle.

1. *Isotropic Conditions:* Under isotropic conditions ($\nu = 0$) and when ϵ increases, the backscatter at a fixed frequency increases and the curve $f \rightarrow \chi(f)$ bends. The angle of insonification does not influence the backscattering coefficient (data are not shown on Fig. 5 for sake of clarity). As shown on Fig. 6, the backscatter at 5 MHz increases with the adhesion energy, reaching a plateau value $\sim 5\chi_{ref}$ (+6.9 dB). The curve bending on Fig. 5 can be quantified by the variations of (n_x, n_y) . The spectral slopes appear on Fig. 7 as a function of the adhesion energy. For $\nu = 0$, their values do not significantly differ. Their value decreases from 4.2 (disaggregated medium) to 3.4 ($\epsilon = 150k_B T$).

TABLE III
BACKSCATTERING PROPERTIES (AND STANDARD ERRORS OF THE MEAN, SEM) AS A FUNCTION OF (ϵ, ν) .

Point process statistical parameters		Scattering properties (mean \pm SEM, $n = 100$, **: $P < 0.001$ paired t -test)			
ν	$\epsilon/k_B T$	χ_x^0/χ_{ref}	χ_y^0/χ_{ref}	n_x	n_y
0	0	0.84 ± 0.06	0.79 ± 0.06	4.21 ± 0.04	4.18 ± 0.04
0	25	3.64 ± 0.23	3.87 ± 0.24	3.53 ± 0.04	3.51 ± 0.04
0	150	4.92 ± 0.33	5.08 ± 0.32	3.39 ± 0.04	3.38 ± 0.04
1	25	1.87 ± 0.14	1.91 ± 0.11	$3.63 \pm 0.04^{**}$	$4.16 \pm 0.04^{**}$
1	150	1.93 ± 0.15	1.84 ± 0.12	$3.54 \pm 0.04^{**}$	$4.21 \pm 0.05^{**}$

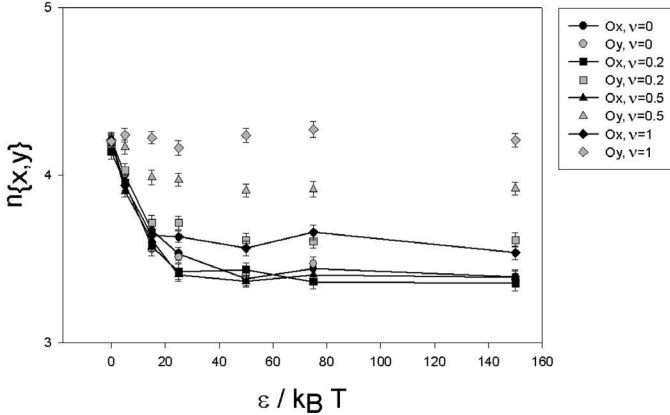


Fig. 7. Spectral slopes in the frequency range 0–40 MHz, in perpendicular (Oy) and in parallel (Ox) with the growth axis as a function of the aggregation potential ϵ and of the anisotropy index ν . The error bars represent the standard error of the mean.

2. *Anisotropic Conditions:* Anisotropic behavior arises when $\nu > 0$. It is revealed on Figs. 5, 7 and in Table III by the angular dependence of the blood scattering properties. For $\epsilon > 0$, the spectral slope along Oy is greater than along Ox (paired t -tests, $n = 100$, $P < 0.001$, for $\nu > 0.2$ and $\epsilon > 0$) as shown on Fig. 7. The difference is more pronounced when either ν or ϵ increases. The slope n_x decreases rapidly with the adhesion energy (similarly to the isotropic conditions), and the decay rate of n_y decreases with ν . For $\nu = 1$, $n_y \sim 4.2$ and slightly depends on ϵ . The angle-independent backscatter at 5 MHz is modulated by the anisotropy as shown on Fig. 6. The plateau value ($\lim_{\epsilon \rightarrow \infty} \chi_z^0/\chi_{ref}$) decreases with ν , falling from 5 (isotropic case) to 1.9 ($\nu = 1$).

IV. DISCUSSION

The feasibility to measure ultrasonically RBC aggregation relies on significative variations of acoustic properties of blood with microstructural variables.

Numerical simulations allow one to select a limited number of physical variables (as particle interaction energies, or medium anisotropy) to assess how they affect the different simulated acoustic features and if they can reliably be inferred from various ultrasound tissue parameters.

In this study, scatterer microstructure was modeled by static statistical distributions (Boltzmann thermodynamic equilibrium). This approach indirectly takes into consideration nonequilibrium shear effects by modulating directly the medium anisotropy and the interparticle adhesive strength.

A. Backscatter at 5 MHz

The backscattering coefficient at 5 MHz was angular independent, as its values perpendicularly and in parallel with the cluster axis were not significantly different. Variations of χ^0 as a function of (ϵ, ν) , therefore, characterize low frequency sensitivity to the overall size of the clusters, independently of their orientation. However, the plateau value $\lim_{\epsilon \rightarrow \infty} \chi^0$ decreases with the anisotropy index ν . This finding seems rather counter-intuitive. However, it must be noted that the parameter ν does not affect only interaction orientation. It also has an effect on the size of the clusters because the morphological characteristics of clusters vary with the interaction ellipse elongation.

The strongest variations of the backscatter as a function of ϵ were observed at low frequency. These results, therefore, show that the presence of aggregation should be detected more easily at low frequency than at high frequency. Foster *et al.* [14] also noticed this decrease of sensitivity when increasing the frequency (in their study of a normal blood, backscatter enhancement due to a shear diminution $32 \text{ s}^{-1} \rightarrow 0.16 \text{ s}^{-1}$ was $+14.3 \text{ dB}$ at 35 MHz and reduced to $+2.9 \text{ dB}$ at 70 MHz). This phenomenon is equivalent to the decrease of the spectral slope with ϵ .

However, the insensitivity of χ^0 to theinsonification angle proves that high-frequency tissue features carry complementary informations on medium microstructure that low-frequency scattering properties cannot measure. For instance, angular information such as the orientation of the main axis of the clusters can be measured only at high frequencies.

B. Spectral Slopes

1. *Isotropic Conditions:* The spectral slopes $\{n_x, n_y\}$ are high-frequency informations that are expected to complete the partial microstructural description provided by

χ^0 . When no aggregation occurs, $n_x = n_y$ and their common value (4.21 ± 0.04) is greater than 4, the theoretical slope expected in the Rayleigh scattering regime [21]. The steric repulsions that induce repulsive correlations on particle positions explain this increased value. Similar results for dense media were already predicted in analytical theoretical studies [21], [31] and were observed in experimental investigations [32], [33].

The increase of ϵ , keeping $\nu = 0$, resulted in a decrease of the spectral slope from 4.21 to 3.4 (Fig. 7). This can be compared to various in vitro blood measurements: Van der Heiden *et al.* [34] measured slope decrease from 3.1 to 1 (along Oy , frequencies 20–40 MHz) for shear rate decreasing from 1000 s^{-1} to 0.02 s^{-1} , and Foster *et al.* [14] demonstrated that the spectral slope between 30 and 70 MHz could fall from 3.5 to 0.4 when the shear rate fell from 32 s^{-1} to 0.16 s^{-1} . The range of variations given by our results, however, is smaller than these experimental values. These discrepancies are probably due to the bidimensionality of the simulations. Three-dimensional spatial patterns generally can adopt many more variable configurations than in 2-D, which possibly affects the range of the acoustical properties.

2. Anisotropic Conditions: The anisotropy of the medium is acoustically revealed by differences existing between n_x and n_y when $\nu > 0$. The parallel slope n_x decreases faster than n_y when anisotropic clusters grow along Ox . Anisotropic backscattering behavior has been reported already in a variety of tissues: blood [15], myocardial fibers [35], skeletal muscle [36], kidney [37], and vessel wall [38]. These studies also suggested that the backscattered power is maximal when the US beam perpendicularly intersects the biggest structures. The experimental study on porcine blood flowing in a stationary Poiseuille flow by Allard *et al.* [15] showed that the maximum Doppler power at 10 MHz is observed for aninsonification angle between 45 and 60 degrees. Anisotropy in the US backscatter, therefore, was also present in this context. Poiseuille flow is characterized by a nonhomogeneous velocity field and shear distribution, so it is difficult to conclude at this point whether the maximal backscatter appeared at an angle perpendicular to aggregate rouleaux.

In the simulation study by Fontaine *et al.* [39] that uses a 2-D particle dynamics approach to document the effect of shear rate on the backscattered power, the angular dependence also was different from present results. The finite beam and nonzero bandwidth of the transmitted acoustic pulse, as considered in [39], likely contribute to this difference of scattering behavior.

3. Propositions for Further Experimental Results: Several new experimental investigations would be of major interest to verify the veracity of these simulation results. The link between the amplitude of adhesive interparticle interactions and the low-frequency backscatter has to be experimentally explored. If such a relation was established, US backscatter could be a new measurement tool for cellu-

lar biophysics and more generally for colloid physics. High-frequency studies (typically 10 to 20 MHz), often limited by attenuation, also need to be performed to verify the angular dependence of the backscatter. Previous results obtained by [15] should be quantified by the backscattering coefficient rather than by the Doppler power, and preferably in a stationary shear flow (Couette system).

V. CONCLUSIONS

A new stochastic approach for modeling the spatial pattern formed by RBCs in blood was proposed in this 2-D study. It enabled us to assess the influence of erythrocyte aggregation (characterized by an adhesion energy ϵ) and rouleaux orientation (anisotropy index ν) on the macroscopic US properties of blood. The frequency and angular dependencies of blood backscatter were characterized by three indices: the (isotropic) backscatter χ^0 at 5 MHz and two spectral slopes (n_x, n_y) in parallel and perpendicular to the growth direction of RBC clusters. The backscatter χ^0 increased with the adhesion strength ϵ . The spectral slope n_x decreased with ϵ while n_y remained nearly constant. This entails that blood backscatter for frequencies ranging between ~ 10 and 40 MHz is more pronounced perpendicularly than in parallel with the aggregate principal axis.

From our results, high-frequency acoustical properties could convey microstructural information (about the anisotropy and elongation of the cell clusters). Three-dimensional simulations in the same controlled aggregating conditions would be useful to precise the sensitivity and variability of the spectroscopic backscatter characteristics to quantitatively infer cell interactions.

REFERENCES

- [1] K. K. Shung and G. A. Thieme, *Ultrasonic Scattering in Biological Tissues*. Boca Raton, FL: CRC Press, 1993.
- [2] M. D. Sherar, M. B. Noss, and F. S. Foster, "Ultrasound backscatter microscopy images the internal structure of living tumour spheroids," *Nature*, vol. 330, no. 6147, pp. 493–495, 1987.
- [3] L. C. Lin, R. F. Yen, J. J. Hwang, F. T. Chiang, C. D. Tseng, and P. J. Huang, "Ultrasonic tissue characterization evaluates myocardial viability and ischemia in patients with coronary artery disease," *Ultrasound Med. Biol.*, vol. 26, no. 5, pp. 759–769, 2000.
- [4] F. Padilla, F. Peyrin, and P. Laugier, "Prediction of backscatter coefficient in trabecular bones using a numerical model of three-dimensional microstructure," *J. Acoust. Soc. Amer.*, vol. 113, no. 2, pp. 1122–1112, 2003.
- [5] S. Chien, "Shear dependence of effective cell volume as a determinant of blood viscosity," *Science*, vol. 168, no. 934, pp. 977–979, 1970.
- [6] R. Fahraeus, "The suspension stability of blood," *Physiol. Rev.*, vol. 9, pp. 241–274, 1929.
- [7] C. Bucherer, C. Lacombe, and J. C. Lelièvre, "Viscosité du sang humain," in *Biomécanique des Fluides et des Tissus Biologiques*. M. Y. Jaffrin and F. Goubel, Eds. Paris: Masson, 1998, pp. 31–51. (in French)
- [8] B. Sigel, J. Machi, J. C. Beitler, J. R. Justin, and J. C. Coelho, "Variable ultrasound echogenicity in flowing blood," *Science*, vol. 218, no. 4579, pp. 1321–1323, 1982.

- [9] A. M. K. Enejder, J. Swartling, P. Aruna, and S. Andersson-Engels, "Influence of cell shape and aggregate formation on the optical properties of flowing whole blood," *Appl. Optics*, vol. 42, no. 7, pp. 1384–1394, 2003.
- [10] T. Chelidze, "Dielectric spectroscopy of blood," *J. Non-Cryst. Solids*, vol. 305, no. 1-3, pp. 285–294, 2002.
- [11] P. C. Johnson, J. J. Bishop, S. Popel, and M. Intaglietta, "Effects of red cell aggregation on the venous microcirculation," *Biorheology*, vol. 36, no. 5-6, pp. 457–460, 1999.
- [12] T. Linde, B. Sandhagen, A. Hagg, C. Morlin, B. Wikstrom, and B. G. Danielson, "Blood viscosity and peripheral vascular resistance in patients with untreated essential hypertension," *J. Hypertension*, vol. 11, no. 7, pp. 731–736, 1993.
- [13] G. D. O. Lowe, A. J. Lee, A. Rumley, J. F. Price, and F. G. R. Fowkes, "Blood viscosity and risk of cardiovascular events: The Edinburgh artery study," *Br. J. Haematol.*, vol. 96, no. 1, pp. 168–173, 1997.
- [14] F. S. Foster, H. Obara, T. Bloomfield, L. K. Ryan, and G. R. Lockwood, "Ultrasound backscatter from blood in the 30 to 70 MHz frequency range," in *Proc. IEEE Ultrason. Symp.*, vol. 3, 1994, pp. 1599–1602.
- [15] L. Allard, G. Cloutier, and L. G. Durand, "Effect of the insonification angle on the Doppler backscattered power under red blood cell aggregation conditions," *IEEE Trans. Ultrason., Ferroelect., Freq. Contr.*, vol. 43, no. 2, pp. 211–219, 1996.
- [16] L. Y. L. Mo and R. S. C. Cobbold, "A unified approach to modeling the backscattered Doppler ultrasound from blood," *IEEE Trans. Biomed. Eng.*, vol. 39, no. 5, pp. 450–461, 1992.
- [17] I. Fontaine, M. Bertrand, and G. Cloutier, "A system-based approach to modeling the ultrasound signal backscattered by red blood cells," *Biophys. J.*, vol. 77, no. 5, pp. 2387–2399, 1999.
- [18] K. K. Shung, R. A. Sigelmann, and J. M. Reid, "Scattering of ultrasound by blood," *IEEE Trans. Biomed. Eng.*, vol. 23, no. 6, pp. 460–467, 1976.
- [19] B. Lim and R. S. C. Cobbold, "On the relation between aggregation, packing and the backscattered ultrasound signal for whole blood," *Ultrasound Med. Biol.*, vol. 25, no. 9, pp. 1395–1405, 1999.
- [20] I. Fontaine and G. Cloutier, "Modeling the frequency dependence (5–120 MHz) of ultrasound backscattering by red cell aggregates in shear flow at a normal hematocrit," *J. Acoust. Soc. Amer.*, vol. 113, no. 5, pp. 2893–2900, 2003.
- [21] P. M. Morse and K. U. Ingard, *Theoretical Acoustics*. Princeton, NJ: Princeton Univ. Press, 1968.
- [22] G. Cloutier and Z. Qin, "Ultrasound backscattering from non-aggregating and aggregating erythrocytes—A review," *Biorheology*, vol. 34, no. 6, pp. 443–470, 1997.
- [23] D. Savéry and G. Cloutier, "Modeling of the acoustic signal backscattered by a biphasic suspension: Application to the characterization of red blood cell aggregation," in *Acoust. Imaging Symp.*. New York: Plenum, 2000, pp. 289–295.
- [24] M. N. M. van Lieshout, *Markov Point Processes and Their Applications*. London: Imperial College Press, 2001.
- [25] D. Savéry and G. Cloutier, "A point process approach to assess the frequency dependence of ultrasound backscattering by aggregating red blood cells," *J. Acoust. Soc. Amer.*, vol. 110, no. 6, pp. 3252–3262, 2001.
- [26] V. Twersky, "Acoustic bulk parameters in distributions of pair-correlated scatterers," *J. Acoust. Soc. Amer.*, vol. 64, no. 6, pp. 1710–1719, 1978.
- [27] C. C. Coussios, "The significance of shape and orientation in single-particle weak-scatterer models," *J. Acoust. Soc. Amer.*, vol. 112, no. 3, pp. 906–915, 2002.
- [28] N. Metropolis, A. Rosenbluth, R. Rosenbluth, A. Teller, and E. Teller, "Equation of state calculations by fast computing machines," *J. Chem. Phys.*, vol. 21, pp. 1087–1092, 1953.
- [29] K. K. Shung, Y. W. Yuan, D. Y. Fei, and J. M. Tarbell, "Effect of flow disturbance on ultrasonic backscatter from blood," *J. Acoust. Soc. Amer.*, vol. 75, no. 4, pp. 1265–1272, 1984.
- [30] J. K. Perkus and G. J. Yevick, "Analysis of classical statistical mechanics by means of collective coordinates," *Phys. Rev.*, vol. 110, no. 1, pp. 1–13, 1958.
- [31] J. F. Chen and J. A. Zagzebski, "Frequency dependence of backscatter coefficient versus scatterer volume fraction," *IEEE Trans. Ultrason., Ferroelect., Freq. Contr.*, vol. 43, no. 3, pp. 345–353, 1996.
- [32] J. A. Campbell and R. C. Waag, "Ultrasonic scattering properties of three random media with implications for tissue characterization," *J. Acoust. Soc. Amer.*, vol. 75, no. 6, pp. 1879–1886, 1984.
- [33] S. H. Wang and K. K. Shung, "An approach for measuring ultrasonic backscattering from biological tissues with focused transducers," *IEEE Trans. Biomed. Eng.*, vol. 44, no. 7, pp. 549–554, 1997.
- [34] M. S. van der Heiden, M. G. de Kroon, N. Bom, and C. Borst, "Ultrasound backscatter at 30 MHz from human blood: Influence of rouleaux size affected by blood modification and shear rate," *Ultrasound Med. Biol.*, vol. 21, no. 6, pp. 817–826, 1995.
- [35] C. S. Hall, M. J. Scott, G. M. Lanza, J. G. Miller, and S. A. Wickline, "The extracellular matrix is an important source of ultrasound backscatter from myocardium," *J. Acoust. Soc. Amer.*, vol. 107, no. 1, pp. 612–619, 2000.
- [36] K. A. Topp and W. D. O'Brien, "Anisotropy of ultrasonic propagation and scattering properties in fresh rat skeletal muscle in vitro," *J. Acoust. Soc. Amer.*, vol. 107, no. 2, pp. 1027–1033, 2000.
- [37] M. F. Insana, "Modeling acoustic backscatter from kidney microstructure using an anisotropic correlation function," *J. Acoust. Soc. Amer.*, vol. 97, no. 1, pp. 649–655, 1995.
- [38] C. T. Nguyen, C. S. Hall, and S. A. Wickline, "Characterization of aortic microstructure with ultrasound: Implications for mechanisms of aortic function and dissection," *IEEE Trans. Ultrason., Ferroelect., Freq. Contr.*, vol. 49, no. 11, pp. 1561–1571, 2002.
- [39] I. Fontaine, D. Savéry, and G. Cloutier, "Simulation of ultrasound backscattering by red cell aggregates: Effect of shear rate and anisotropy," *Biophys. J.*, vol. 82, no. 5, pp. 1696–1710, 2002.



David Savéry was born in November, 1975 in Lannion, Brittany, France. He graduated from the École Nationale Supérieure des Mines de Paris, Paris, France, in 1998, majoring in image analysis and image processing. During undergraduate studies, he worked at the Centre de Morphologie Mathématique, École des Mines de Paris, Fontainebleau, France, on the characterization of heterogeneous media, using stochastic geometry to model materials microstructure. In 1998, he joined the Laboratory of Biorheology and Medical Ultrasonics, University of Montréal Hospital, Montréal, Canada, where he received his Ph.D. in biomedical engineering in 2003. His research there focused on the modeling of ultrasound scattering by blood.

David Savéry is currently a senior member of the research staff at Philips Research USA, Briarcliff Manor, NY. His research interests are in statistical signal processing, medical imaging, ultrasound tissue characterization, biomechanics and statistical physics of condensed matter.



Guy Cloutier (S'89–M'90) obtained his B.Eng. degree in electrical engineering from the Université du Québec à Trois-Rivières, Trois-Rivières, Québec, Canada, in 1983, and his M.Sc. and Ph.D. degrees in biomedical engineering from the École Polytechnique of Montréal, Montréal, Québec, Canada, in 1986 and 1990, respectively. Between 1990 and 1992, he pursued a postdoctoral training with Dr. K. Kirk Shung at the Laboratory of Medical Ultrasonics, Bioengineering Program, The Pennsylvania State University, University Park, PA.

Dr. Cloutier is currently director of the Laboratory of Biorheology and Medical Ultrasonics at the Research Center of the University of Montreal Hospital, Member of the Institute of Biomedical Engineering of the École Polytechnique at the University of Montreal,

and professor in the Department of Radiology, Radio-oncology, and Nuclear Medicine, Faculty of Medicine, University of Montreal.

His research interests are the characterization of red blood cell aggregation dynamics with ultrasound and rheological methods, the 3-D morphologic and hemodynamic assessment of lower limb arterial stenoses with radiological imaging methods, the characterization of the biomechanical properties of vascular wall structures with ultrasound elastography, and mathematical and biomechanical modeling. He has published more than 70 peer-reviewed papers and book chapters in these fields; he is a member of the advisory editorial board for the journals "Ultrasound in Medicine and Biology" and "Current Medical Imaging Reviews"; and he served on several grant review study sections of the Heart and Stroke Foundation of Canada, the Canadian Institutes of Health Research, the Fonds de la Recherche en Santé du Québec (FRSQ), the Canada Research Chairs, and the National Institutes of Health of USA. Dr. Cloutier is the recipient of a National Scientist award from FRSQ (2004-2009).